Submarine landslides along the Malacca Strait-Mergui Basin shelf margin: Insights from sequence-stratigraphic analysis

Yu-nung Nina Lin,[1] Kerry Sieh,[2] and Joann Stock[1]

Received 14 October 2009; revised 15 June 2010; accepted 21 July 2010; published 2 December 2010.

[1] The enormously destructive tsunami of December 2004, caused by sudden motion of the Sunda megathrust beneath the Indian Ocean, raised concerns about tectonically induced tsunami worldwide. Submarine landslides may also trigger dangerous tsunami. However, the potential and repeat time for such events is in most places poorly known due to inadequate exploration of the sea floor and age constraints. The high sediment flux and tectonic subsidence rate of the Malacca Strait-Mergui Basin shelf margin NE of northernmost Sumatra provide a favorable environment to generate and preserve submarine landslides. From ten seismic reflection profiles acquired in 2006, we identify three sediment packages that exhibit sliding characteristics such as headscarps, distorted beds and debris-toe structures. We assign lowstand marine isotope stages to the paleo-shoreline indicators observed in the profiles. We then determine the ages of these submarine landslides as 20–30 ka, 342–364 ka and 435–480 ka by the paleo-shoreline indicators that bound the top and bottom of the slide bodies. This sequence-stratigraphic approach shows that these events occurred near times of sea-level lowstands, which implies that a large amount of direct sediment influx during glacial periods is an essential precondition for basin-margin submarine landsliding. Spatiotemporal variations of sediment input due to lobe switching or Asian monsoon intensity changes also control basin-margin instability. Because we are currently at a highstand stage, and sediment flux to the continental margin is relatively small, so the chance of having a repeat submarine landslide and landslide tsunami along this basin-margin is low.

Citation: Lin, Y. N., K. Sieh, and J. Stock (2010), Submarine landslides along the Malacca Strait-Mergui Basin shelf margin: Insights from sequence-stratigraphic analysis, *J. Geophys. Res.*, *115*, B12102, doi:10.1029/2009JB007050.

1. Introduction

[2] The disastrous Indian Ocean tsunami of 2004 suggests that tsunamis are potentially among the greatest of natural disasters. Among the various types of tsunami, those generated by submarine landslides are perhaps the most poorly understood in terms of past and potential sizes, frequency and location. Only a few rare events are relatively well known (for example, see *Evans et al.* [2005] for a discussion of paleoslides along the Atlantic continental margin of NW Europe). Because most paleoslides occur along continental slopes, it is plausible to use sequence stratigraphic methodology to determine event ages, geometries and sizes.

[3] The Malacca Strait-Mergui Basin shelf margin (Figure 1) offers just such an opportunity. The −125 m contour, the approximate sea level of the last glacial maximum (LGM) about 21 kyr ago, demarcates the approximate shelf margin. Between Sumatra and the Malay Peninsula, this contour marks the LGM transition from shallow fluvial surfaces to the southeast and the steeper continental slope to the northwest. With high fluvial sediment influx and a substantial subsidence rate, the opportunity for creation and preservation of landslides is optimal; in fact, we find paleolandslide sequences preserved within the sediments of the shelf margin.

[4] By pairing successive paleo-shoreline indicators with lowstand marine isotope stages (MIS), we have determined the ages of the paleoslides. This yields an understanding of the relationship between landslide timing and glacial cycles. This correlation in turn allows us to make meaningful statements about the likelihood of future catastrophic landslides in this region.

2. Geologic and Hydrographic Setting

[5] Mergui Basin is a Tertiary marine graben formed by post-Oligocene normal faulting. Back-arc spreading in the Andaman Sea first started from this region and formed a series of NE–SW striking transtensional structures and the basin outline (Figure 1b; *Curray* [2005]). The locus of rifting has been continuously shifting westward since Early Miocene time, leading to a deceleration of subsidence in the Mergui Basin. The most recent phase of subsidence in the

[1]Geological and Planetary Sciences, California Institute of Technology, Pasadena, California, USA.
[2]Earth Observatory of Singapore, Nanyang Technological University, Singapore.

0148-0227/10/2009JB007050

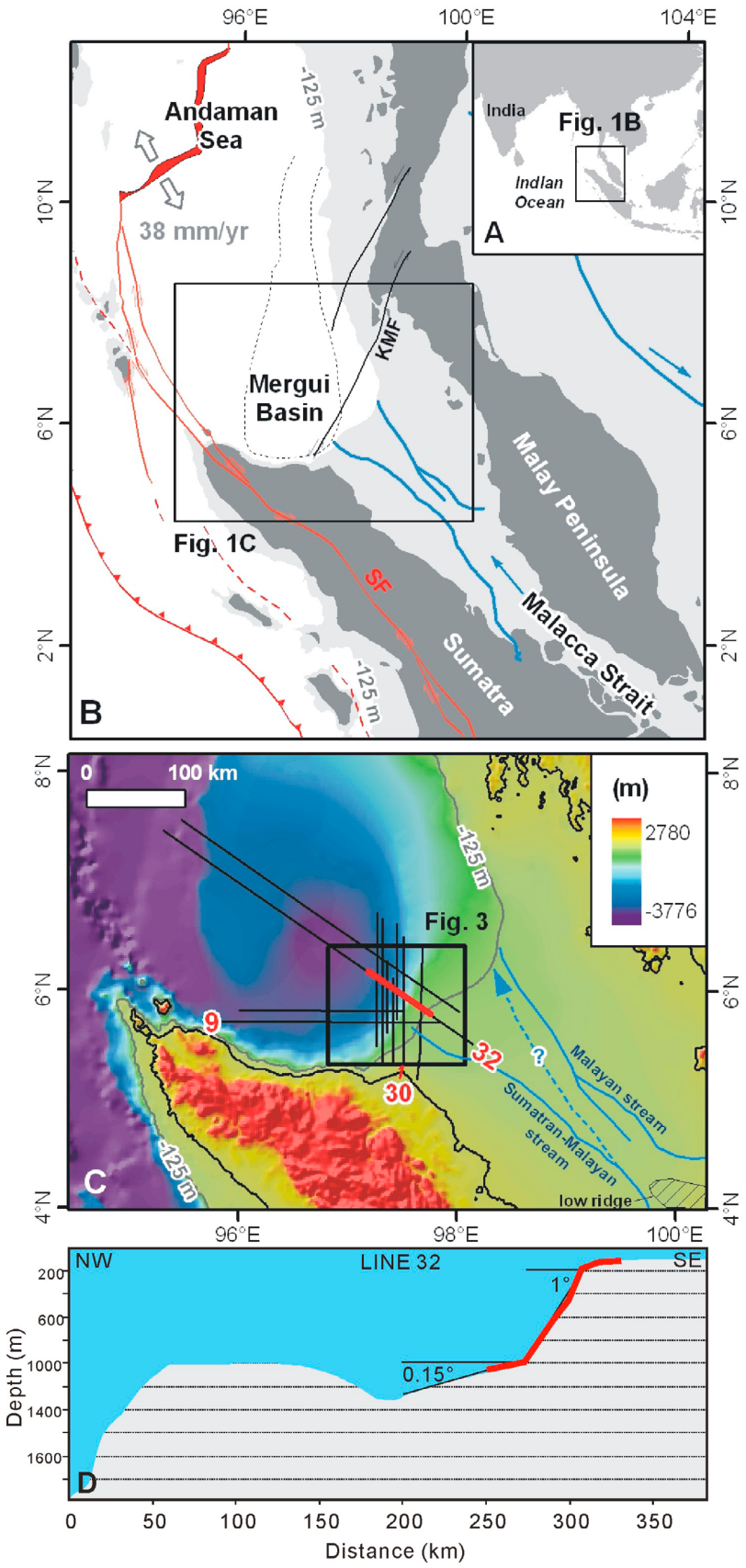
96°E
100°E
104°E
10°N
6°N
2°N
Andaman Sea
38 mm/yr
-125 m
India
Fig. 1B
Indian Ocean
A
Mergui Basin
KMF
Fig. 1C
SF
Sumatra
Malay Peninsula
Malacca Strait
B
8°N
4°N
0
100 km
(m)
2780
-3776
Fig. 3
9
32
30
Malayan stream
Sumatran-Malayan stream
low ridge
C
96°E
98°E
100°E
NW
LINE 32
SE
1°
0.15°
Depth (m)
200
600
1000
1400
1600
D
0
50
100
150
200
250
300
350
Distance (km)

Figure 1

Andaman Sea has been the fast opening of the current Andaman Sea spreading center, which began ~4 Ma and continues today [*Kamesh Raju et al.*, 2004]. Given this approximate onset age, we can estimate the subsidence rate of the latest phase based on the offset of the Late-Miocene unconformity by normal faults (Appendix A). This gives us an average rate of 0.25 mm/yr, with the rate for the southern basin as high as 0.3–0.35 mm/yr. The high subsidence rate, one order of magnitude higher than the rate of ~0.015–0.03 mm/yr in the West Indian Ocean passive continental margin [*Whiting et al.*, 1994], is creating a large accommodation space for accumulation of sediments.

[6] Bathymetry, 3.5 kHz echo-sounder records and sub-bottom information [*Emmel and Curray*, 1982], reveal that sediments have been transported into the basin by two major stream systems in the Malacca Strait since at least 150 ka. Rivers coming off the Malay Peninsula between 3–4°N joined a major Sumatran river and flowed northwestward through a single valley. This bigger drainage system is called the Sumatran-Malayan stream. The rivers draining the Malay Peninsula between 4–5.5°N, called the Malayan stream, are separated from the Sumatran-Malayan stream by a low ridge (Figure 1c). The volume accumulation rate of sediment from both streams has averaged as high as 3.9×10^5 km^3/myr for the past 2 Myr [*Métivier et al.*, 1999]. This rate results from the proximity to land masses as well as high tropical denudation rates (order of 0.1–1 cm/yr; *von Blanckenburg et al.* [2004]). The enormous sediment supply, together with the large accommodation space created by normal faulting, make the Malacca Strait-Mergui Basin shelf margin a perfect place to study sequence stratigraphy and submarine landslide processes.

3. Submarine Landslide Texture and Geometry

[7] We studied ten industry seismic reflection profiles that were acquired in 2006 by the 2D seismic survey vessel M/V Zephyr using a 3050 in^3 sleeve gun array source. Data were recorded on an 8000-m streamer with group interval of 12.5 m and a sample rate of 2 msec. Seismic lines spanned the shelf margin from water depths of 80 m to below 1000 m (Figure 1c). Data were processed by surface-related multiple elimination (SRME) and Radon demultiple, followed by prestack time migration up to 6 seconds, and then down-sampled to 4 msec resolution. We carried out a simple time-depth conversion by assuming seismic velocity of 1600 m/s near the sea floor to 1800 m/s at 2 seconds beneath the sea floor. These velocities are based on the check shot velocity analysis from a borehole on the other side of the Sunda Shelf, near the Natuna Islands (water depth 60 m; unpublished industrial report). We generated the time-depth chart in the Kingdom suite software and executed the simple time-depth conversion. This velocity model will introduce errors into the depth and volume estimates of the whole analysis. Without any drillhole verification, however, it is difficult to quantify the magnitude of errors. The following analysis is restricted to the 0–2 second two way travel time window.

[8] Through loop correlation among these ten lines, we identify three meso-scale landslides (LS1, LS2 and LS3 in Figure 2). These paleoslides and associated debris lobes exhibit highly diffracted seismic reflections caused by high-angle tilted beds within the slump bodies and irregular slump top surfaces. These slump tops are also characterized by strong reflections due to the difference in acoustic impedance between the slide body and overlying materials (Figure 2a). The lack of continuous and smooth reflectors within slide bodies implies considerable internal deformation within the deposit, rather than pure block translation.

[9] All three paleoslides have a similar geometry. Headscarp heights range between 200 and 300 m, with scarp slopes of 9° to 25° (Table 1). Glide planes range from 39 to 65 km in length, on slopes of 0.3° to 1.1°. Slump blocks, irregular glide-plane bases, long debris lobes and debris toes characterize all three paleoslides. The oldest slide, LS1, has very steep headscarp slope and encompasses large slumping blocks near the proximal region of the slide body (Figures 2, 3 and Table 1). LS2 is composed of multiple subslides (see details in Appendix B). The original headscarp of the major slides has been erosionally removed by two later retrogressive events (Figure 3). The youngest paleoslide, LS3, has the largest area, largest volume and highest headscarp. It also has a debris lobe up to 75 km long, which may also indicate high transport velocity. LS2 and LS3 are southwest of LS1, perhaps because of migration of the main fluvial channel.

4. Landslide Age Determination

[10] In addition to the three landslide bodies, other prominent features in these seismic profiles are the paleo-shoreline indicators (*Rabineau et al.* [2005, 2006] clearly identify the same geometry in the Gulf of Lion). Paleo-shoreline indicators are characterized by sharp northwestward steepening of dip angles on continuous top reflectors (Figure 2a), representing the topset-to-foreset transitions of older buried delta lobes [*Asku et al.*, 1999]. In our seismic reflection profiles, southeastward of these points, steeper inclined reflectors are truncated by sub-horizontal top reflectors, which represent subaerial erosional surfaces of a forced regression. Gravity core observations in the Malacca Strait-Mergui Basin also verify an alluvial-delta-fan system

Figure 1. Location and bathymetry of the Malacca Strait-Mergui Basin shelf margin within the context of the Indian Ocean (A) and its simplified submerged drainage system in thick blue lines (B, modified from *Emmel and Curray* [1982]). The −125 m contour delimits the coastline during last glacial maximum. Red lines are the Sunda Trench and other active structures, including the Sumatran Fault (SF) [*Singh et al.*, 2008]. The Andaman Sea spreading center has been spreading at 38 mm/yr since 2 Ma [*von Blanckenburg et al.*, 2004]. Inactive Miocene strike-slip faults are black (KMF: Khlong Marui Fault). Pre-Pliocene basement highs delineate the boundary of the Mergui Basin (dotted black lines). Structures and basin boundary are from *Curray* [2005]. (C) Bathymetry of the Malacca Strait-Mergui Basin shelf margin from ETOPO 1 (1′ resolution) and eleven seismic profiles used in this study. Line 32 of Figure 2 is red. (D) Bathymetry profile along the entire length of Line 32, derived from ETPOP 1 data. Red segment corresponds to the part of Line 32 shown in Figure 2.

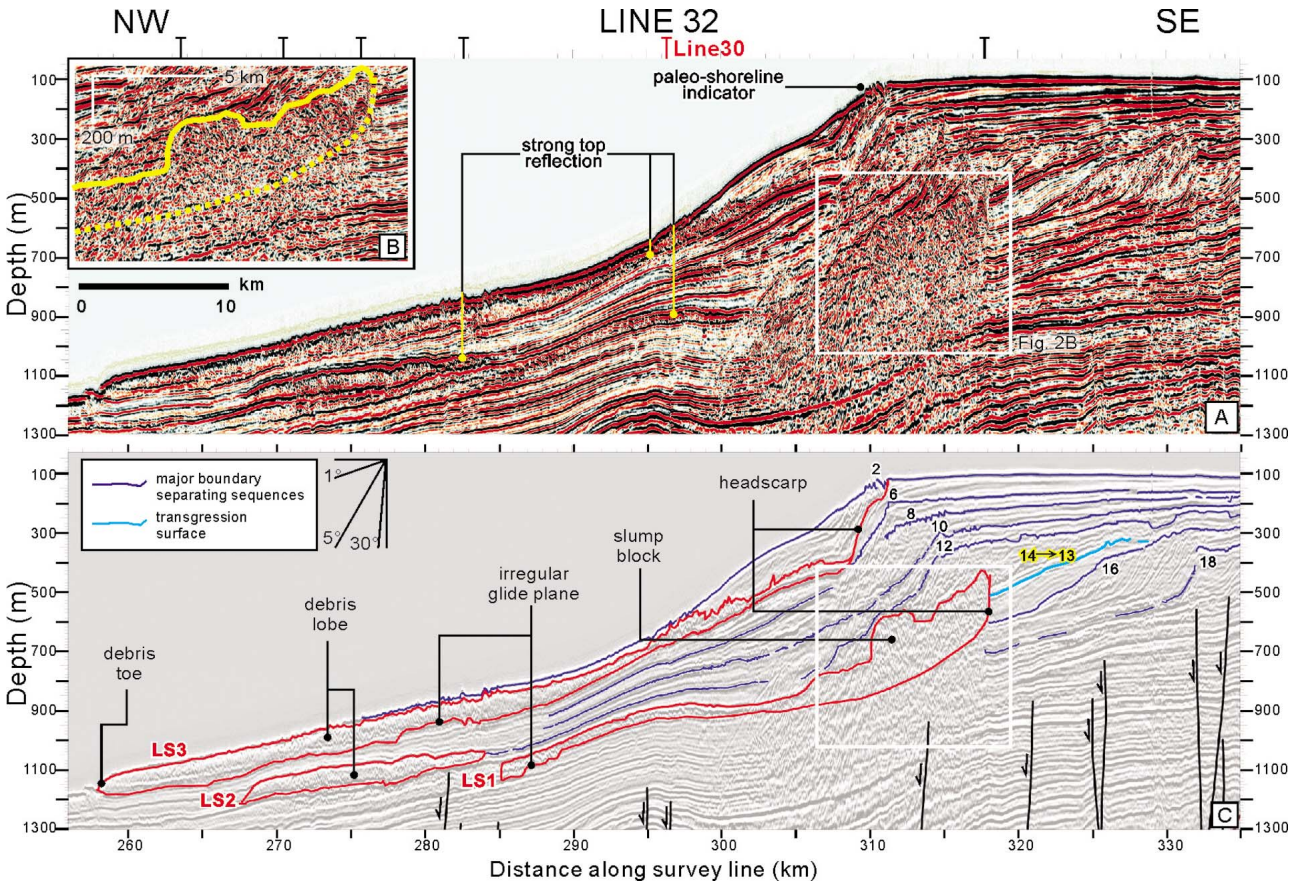

Figure 2. (a) Seismic profile Line 32 in depth (see position on Figure 1), with 20× vertical exaggeration. Nails at the top of figure mark the intersection of Line 32 with other profiles used in loop correlation. (b) Enlargement of a portion of Line 32 (white box in Figure 2a) that displays a landslide, with 10x vertical exaggeration. Yellow solid line represents the landslide top, defined by the boundary between continuous and discontinuous reflectors. Yellow dashed line indicates the landslide base, which is less clear because of interference by diffractions from disturbed overlying material. (c) Interpreted seismic profile of Figure 2a. Thick red lines outline three landslides (LS1, LS2 and LS3). Boundaries between transgressive and regressive sequences are dark blue lines; pale blue line is the transgression surface during the long transgression period from marine isotope stage (MIS) 14 to 13 (see sea-level curves in Figure 4). Paleo-shoreline indicators correspond to the inflection points on the sequence boundaries and are correlate with marine isotope stages (black numbers).

during LGM [*Emmel and Curray*, 1982]. Basinward of these points, the top reflectors are concordant with the underlying reflectors, indicating continuous subaqueous deposition. This dip-angle transition point therefore represents the land/ocean boundary during lowstands, when the shoreline retreats to this part of the Malacca Strait-Mergui Basin continental shelf, with its timing corresponding to a glacial maximum. Thus, the top reflector is a major boundary separating regressive and transgressive sequences. We identify seven of these paleo-shoreline indicators in the three profiles normal to the shelf margin (from north to south, Line 35, 32 and 9; Figures 1c and 2c).

[11] If there was no lobe switching beyond the limits of the profiles through the time these sequences were depos-

Table 1. Summary of Landslide Age, Characteristic Features and Geometry

	Age (ka)			Headscarp		Glide Plane[b]			
	Tmin[a]	Tmax[a]	Headscarp Feature	Height (m)	Slope (°)	Length (km)	Slope (°)	Area (km^2)	Volume (km^3)
LS3	20 (2.2)	30 (3.0)	Multiple (major + small scarps)	>280	9	65	0.9	~1,465	~75
LS2 (retrogressive)	250 (8.2)	287 (8.5)	multiple	>210	24	17	0.8	~50	~7
LS2 (major)	342 (10.2)	364 (11.0)	erosionally removed	N/A	N/A	>40	0.3	>630	>34
LS1	435 (12.2)	480 (13.1)	single scarp	>250	25	39	1.1	~960	~65

[a]Number represents age; number in parentheses represents corresponding marine isotope stage [MIS; from *Prell et al.*, 1986].
[b]Glide plane lengths and slopes were measured on seismic lines.

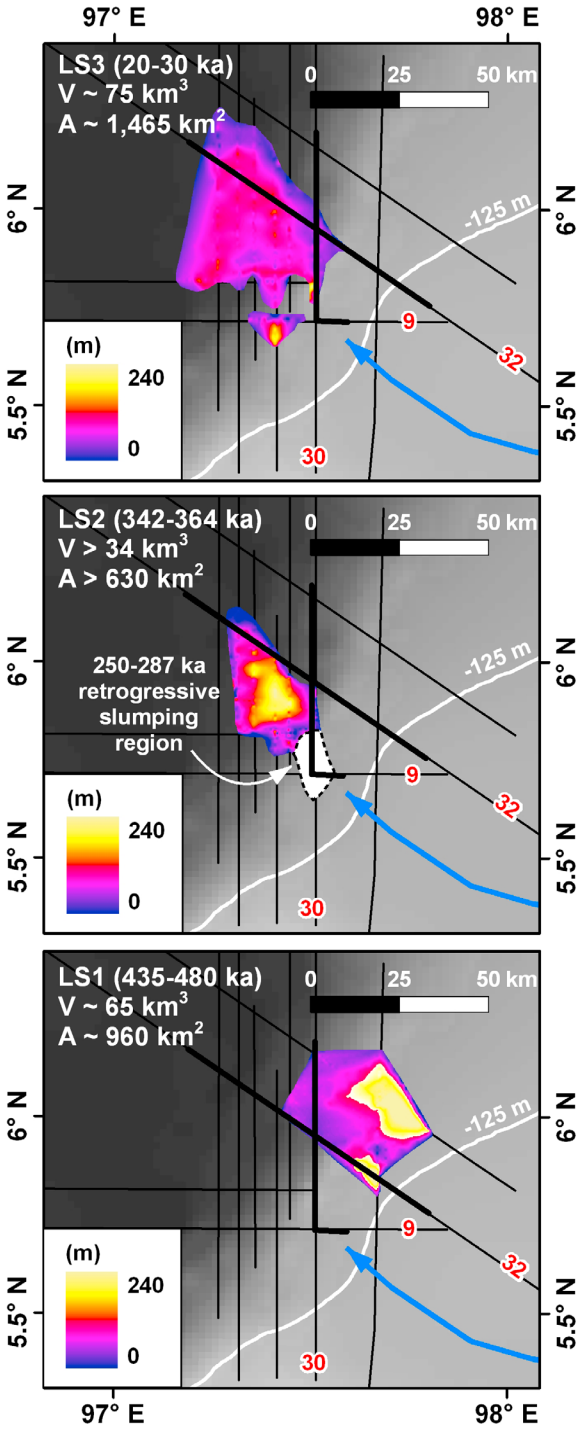

Figure 3. Thickness maps of the three paleoslides (see map position on Figure 1c). Black seismic lines indicate all profiles used to determine slide thickness and extent. Heavier black lines show extent of seismic images for Line 32, 30 and 9 (Figures 2 and A2). We constrain their ages by the paleo-shoreline indicators that bound their tops and bottoms. Note the volume and area for LS1 are less well determined because the constraining profiles are farther apart. The calculated volume of LS2 includes only the volume of the major subslide (see Appendix B). The southwestward migration of the landslides through time may indicate the migration of the major channel.

ited, then no sequence is missing in these profiles (we will revisit this assumption in section 5.1). If this is correct, then we may assign marine isotope stages (MIS) sequentially to these paleo-shoreline indicators (Figure 2c). To determine the most reasonable age model for each of these paleo-shoreline indicators, we convolved relative sea-level curves with local tectonic subsidence rates. We also corrected for sediment compaction according to the observed depth of these paleo-shoreline indicators, in order to remove the effect of compactional deepening. Thus we are able to assign paleo-shoreline indicators to sea-level minima on the relative sea-level curves, accounting for subsidence rates from 0.4 mm/yr in the north (Line 35) to 0.65 mm/yr in the south (Line 9) (Figure 4). These subsidence values are within the same order of magnitude as the average post-4-Ma subsidence rate for this basin that we calculated above (~0.25 mm/yr). That the modeled rates are higher in the southern part is also consistent with the southward deepening of the Late-Miocene unconformity in the Mergui Basin (Appendix A).

[12] Although we assume that there was no lobe switching to positions outside of the area of our seismic lines throughout the period of deposition of the sediments, it is possible that one or more paleo-lowstands did not prograde as far to the northwest as our lines. It is also possible that one or more periods of forced regression were too short for a clear regression sequence to develop. Such is the case of the short regression from MIS 15 to 14, which was followed by a long transgression from MIS 14 to 13 (Figure 4). The apparently longer transgression time span may explain the thick moderately-dipping sequence atop the MIS 16 sequence boundary, which is not typical of forced regression foresets. We interpret this unit as the transgression sequence and the top is interpreted as the transgression surface from MIS 14 to 13 (Figure 2c).

[13] We build two scenarios regarding the order of occurrence of submarine landsliding and transgression/regression events (Figure 5). In scenario I, the landslide occurs during a regression period. After this sliding, the regression sequence continues to propagate outward and the paleo-shoreline indicator is preserved. Considering that the Malacca Strait-Mergui Basin shelf margin is located close to lowstand sea levels, the timing should be close to the end of regression (peak glaciation) rather than in the middle of the long regression. This geometry is observed in LS1 and LS3 in most of our seismic profiles (Figure 2).

[14] In scenario II, the landslide occurs during transgression. According to 3.5 kHz eco-sounder data acquired in the 70's [*Emmel and Curray*, 1982], about 20–30 m of sediment accumulated between the LGM old sea floor and modern sea floor near the outlet of the Malacca Strait. This sediment package represents the transgressive tract from MIS 2 to present day (MIS 1). The relative sea-level curve shows that the rate of sea level rise during each transgression period within the past 600 kyr is quite similar to the rate during the last transgression, except for the long transgression from MIS 14 to MIS 13 (Figures 2 and 4; the package of more gently inclined layers embedded between more steeply inclined sediment packages). This suggests that the transgression sequence thickness is usually about 20–30 m thick around the strait outlet. Given the thin transgression sequence, if a landslide occurs during transgression period,

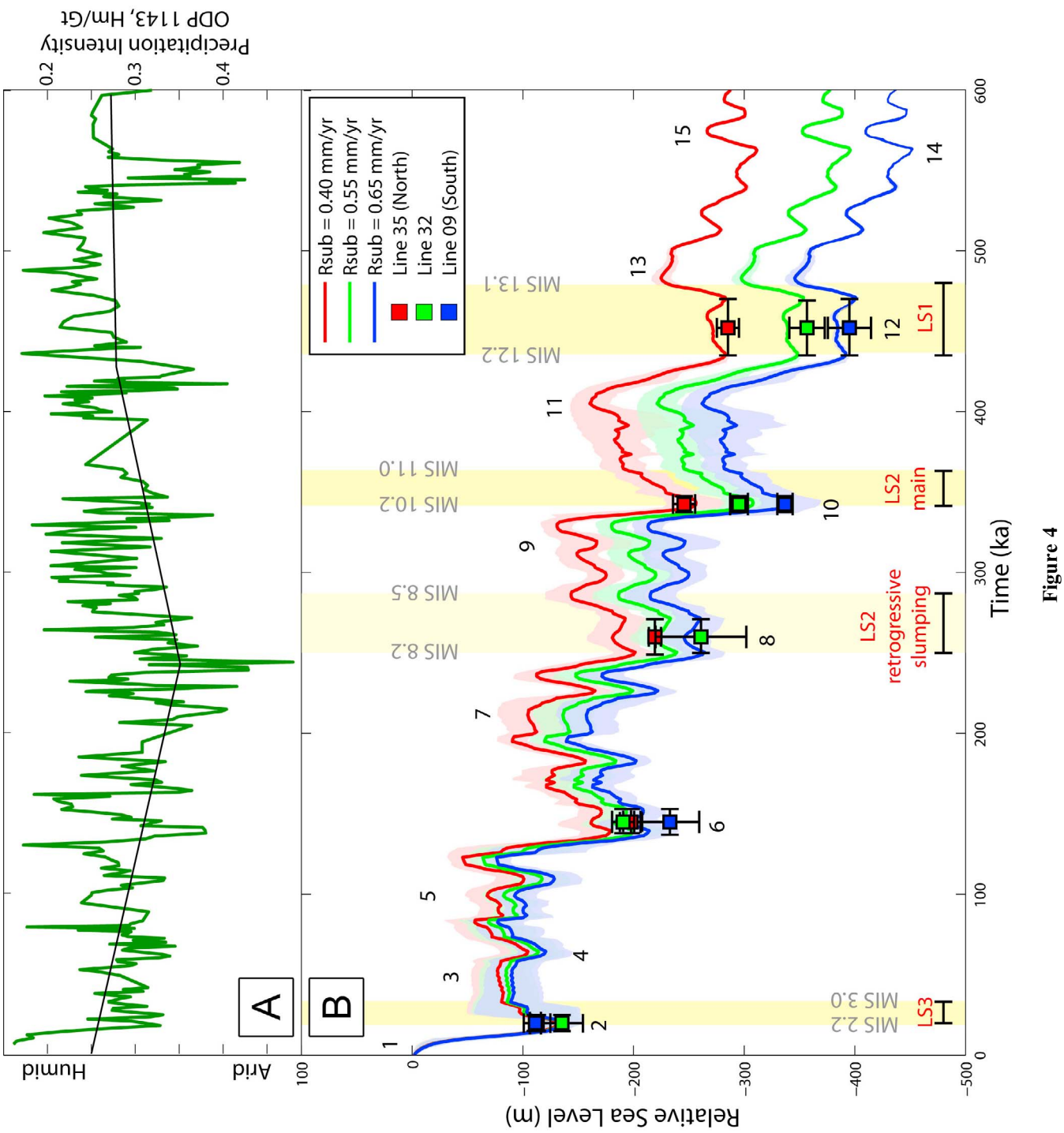
Precipitation Intensity
ODP 1143, Hm/Gt
0.2
0.3
0.4
A
Arid
Humid
B
Rsub = 0.40 mm/yr
Rsub = 0.55 mm/yr
Rsub = 0.65 mm/yr
Line 35 (North)
Line 32
Line 09 (South)
MIS 13.1
MIS 12.2
MIS 11.0
MIS 10.2
MIS 8.5
MIS 8.2
MIS 3.0
MIS 2.2
LS3
LS2 retrogressive slumping
LS2 main
LS1
1
2
3
4
5
6
7
8
9
10
11
12
13
14
15
Relative Sea Level (m)
Time (ka)
100
0
−100
−200
−300
−400
−500
0
100
200
300
400
500
600

Figure 4

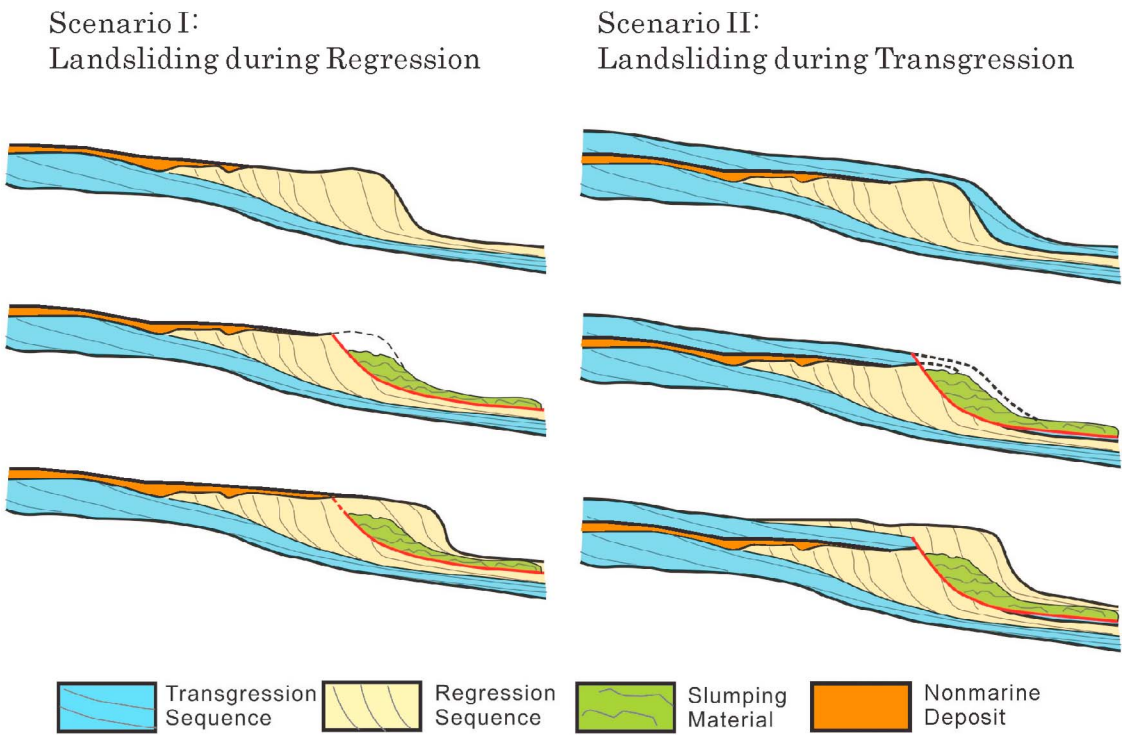

Figure 5. Scenarios regarding the order of occurrence of submarine landsliding and transgression/regression events. Stratigraphic sequence is adapted after *Rabineau et al.* [2005]. See text for detailed discussion of these scenarios.

the top of the slide body is more likely to fall below the previous regression surface. In this case the paleo-shoreline indicator of the previous regression event will be eroded as well. In the case of LS2, its headscarp eroded away the paleo-shoreline indicator of MIS 10, as expected in scenario II (Appendix B). However, the top of the slide body is much higher than the regression surface of MIS 10. LS2 therefore more likely occurred during regression to MIS 8. Based on this interpretation, we believe that the three major events that we observe all occurred during regression.

[15] We now date the three paleoslides by using the bounding paleo-shoreline indicators. Their upper age bounds are set to the glacial maxima represented by the overlying paleo-shoreline indicators. Because the slide headscarps cut through the regression sequences on the shelf margin rather than somewhere in the strait, these slides occurred while sea levels retreated to almost lowstand. We therefore narrow down the lower age bounds to the closest regression substages before the glacial maxima (Figure 4). This gives the approximate ages of 435–480 ka, 342–364 ka and 20–30 ka for LS1, LS2 (main event) and LS3 respectively (Table 1).

5. Discussion

5.1. Source of Uncertainties

[16] Since the normal fault system along the basin margin may have been active since ~4 Ma, we further consider the influence of any normal faulting on the paleo-shoreline indicators. The estimated 0.25–0.35 mm/yr subsidence rate of the last 4 Ma would have created an extra accommodation space due to subsidence of about 25–35 m per 100 kyr. This accommodation space would have been distributed along a wide normal fault system (Appendix A), so the space related to each individual fault could be small and can be ignored. If, by any chance, the tectonic subsidence rate along one specific fault were larger than average during a specific time period and thus created extra accommodation space, two scenarios would be plausible. The first scenario is that a new paleo-shoreline indicator, representative of the sea level at

Figure 4. (a) Asian monsoon precipitation intensity, derived from the ratio of hematite (Hm) to goethite (Gt) of ODP Site 1143 for the last 600 kyr. The black straight lines represent the long-term trend of the records [*Zhang et al.*, 2007]. (b) Relative sea-level curves, after combining the eustatic sea-level curve and tectonic subsidence rates (red, green and blue lines are 0.4–0.65 mm/yr). Error ranges of these curves derive from multiple sea-level sources (from isotopic curves, glacio-isostatic modeling, stratigraphic modeling or point measurements such as corals) assembled by *Rabineau et al.* [2006]. Paleo-shoreline indicators frome this study (squares) are corrected by decompaction to restore their depositional depth. Abscissa errors are determined by the length of corresponding lowstand periods; ordinate errors are the uncertainties in measuring the depth of paleo-shoreline indicators on the seismic section. Numbers in black: MIS stages. Bounding MIS substages of each landslide are after *Prell et al.* [1986].

that time, would have been formed above the old paleo-shoreline indicator. Since the regression surface reflector is contiguous with the new paleo-shoreline indicator, we could still identify the correct paleo-shoreline indicator and make the linkage to MIS. The second scenario is that the sedimentation rate was not able to catch up with the pace of subsidence. The regressive foresets would have formed over the submerged block but would not have fully filled the accommodation space. Even if this happened, since the post-faulting foresets would be progradationally contiguous across the fault, a new paleo-shoreline indicator would still be formed around the sea level, atop the old paleo-shoreline indicator. In this case, we can distinguish which paleo-shoreline indicator is representative of the sea level by tracing the continuity of foresets. From these two scenarios, we conclude that in the passive continental margin, when carefully identified, paleo-shoreline indicator is a robust proxy of sea levels and thus marine isotope stages.

[17] Now we come back to our assumption of no significant lobe-switching. Lobe-switching is the norm for most sedimentary systems, and the delta at the outlet of the Sumatran-Malayan stream should be no exception. However, since our study area covers over half of the Malacca Strait-Mergui Basin shelf margin, we assume that our data encompass most of the lobe-switching events. If the lobe did switch outside our study area in the past, as shown in Figure 1c, one or more cycles of system tracts will be partially or totally missing in our seismic lines. This scenario means part of our paleo-shoreline indicators could be off by one or two glacial cycles and should be moved backward in time. If this were true, our obtained subsidence rate would have been over-estimated. The age of the paleoslides will also be off by one or two glacial cycles.

[18] The third source of uncertainty, and potentially a big one, comes from our seismic velocity model. As mentioned before, we apply a single time-depth conversion function to all our seismic profiles, even though sediment type surely changes from shelf margin to basin center and this should be accompanied by changes in seismic velocity. Advanced velocity analysis can greatly reduce this error, but we do not have the raw seismic data that would allow us to carry out such a sophisticated analysis. Fortunately, even with our current rough velocity model, it is unlikely that landslide volume will be off by a factor of two, since our velocity model is still constrained by a drillhole. Still, we caution that the subsidence rates may be different than what we have estimated.

5.2. Causes of Landslides

[19] One of the best-studied submarine landslides provides some insights regarding plausible mechanisms for ours. The Storegga slide occurred on the continental slope west of Norway about 8200 years BP and is among the largest known [*Bugge et al.*, 1987, 1988; *Haflidason et al.*, 2003, 2004; *Bryn et al.*, 2005; *Kvalstad et al.*, 2005]. Many factors appear to have contributed to causing the slide. The existence of a weaker layer (a "contourite") may have been critical to the initiation of sliding [*Laberg et al.*, 2003; *Kvalstad et al.*, 2005]. Nonetheless, a contourite by itself is not enough to induce failure, because rapid loading of glacial sediments over the water-rich contourite is what would raise pore pressure in the contourite to initiate a slide. *Bryn et al.* [2005] therefore proposed that the glacial cycle is another key factor that controls where and when a slide occurs. Even so, calculations suggest that seismic shaking would still have been required to trigger the landslides [*Bryn et al.*, 2005; *Kvalstad et al.*, 2005]. Thus, studies of the Storegga slide imply a complicated trigger that involves both a long-term, stratigraphic precondition and a short-term, seismic event.

[20] What might have been the preconditioning for the Malacca Strait-Mergui Basin submarine landslides? All occurred during periods of low sea level, so one might propose conditions related to sea-level lowstands. This implies that slumping occured when sediments were being deposited in copious amounts directly onto the shelf margin. Such rapid accumulation would likely result in high pore pressures in poorly consolidated, young strata. Supporting this hypothesis is the observation that on the other side of the Malay Peninsula, along the Sunda shelf margin between Vietnam and Borneo, the mass accumulation rate during the LGM was almost three times as much as the rate in Holocene [*Wang*, 1999]. *Wang* [1999] attribute this big difference of mass accumulation not only to the direct fluvial discharge onto the shelf, but also to erosion of the newly exposed shelf by the currently submerged paleo-Sunda river. A large amount of direct sediment influx might therefore be the most essential precondition for a submarine landslide to occur along the Malacca strait-Mergui Basin shelf margin.

[21] Another precondition for large failures of the Malacca Strait-Mergui Basin shelf margin might be regionally uniform parallel bedding, as seen in seismic profiles (Figures 2 and A2). Parallel-bedded sediment sequences with little variability over large areas characterize their sub-surface structure, with the result that, should the conditions for slope failure occur, they can simultaneously affect large areas [*Masson et al.*, 2006]. Existence of clay-rich layers can further enhance the possibility of large failures, since pore overpressure and time-dependent strain in such layers can create potential slide surfaces of low frictional strength [*O'Leary*, 1991]. A lack of scientific boreholes in the region stymies any test of weak layers at the moment. Nonetheless, this is plausible because substrate sediments in the outlet of the Malacca Strait are dominated by muddy sand and sand with local concentrations of mud [*Keller and Richards*, 1967; *Emery*, 1971]. One can speculate that this irregularly distributed mud created an impermeable low friction layer that became the slide surfaces.

[22] Although it likely played a decisive role, direct sediment influx associated during global glacial maxima cannot be the only controlling factor for basin-margin instability, because we do not see large landslides during every glacial maximum. Perhaps there are factors that produce spatio-temporal variations in sediment supply and hence landslide occurrence. One factor could be deltaic lobe switching, that is, channel migration, within the study area. Note that we see a southward temporal migration of the slides, with the youngest slide, LS3, at the youngest submerged outlet of the Sumatran-Malayan stream. Perhaps landslides happen on the specific part of the continental slope for which we have data only after the river has dumped large volumes of sediment there. To test that idea, we would need a more detailed grid of 2D seismic lines or (or 3D seismic volume) to

construct a complete story of drainage evolution through the past few glacial cycles.

[23] We also propose another reason for spatiotemporal variation in landsliding: long-period variations in Asian monsoon intensity. A higher intensity of the Asian monsoon causes more precipitation leading to higher erosion rates and concomitantly higher rates of sediment influx [*Métivier et al.*, 1999]. According to *Zhang et al.* [2007], Asian monsoon intensity decreased from 400 ka to 250 ka and then increased from 250 ka to present (Figure 4). This long-period variation seems to correlate with the decrease in size of both the main and retrogressive events of LS2 and the longer period between LS2 retrogressive events and LS3 (Figure 4). Based on this temporal correlation, basin-margin instability in this region may be coupled with long-term ENSO variations.

[24] Even with all these preconditions and spatiotemporal variations, strong seismic shaking may still be required to trigger these landslides. The need for such a short-term trigger has been suggested in the cases of Storegga [*Kvalstad et al.*, 2005] and volcanic island collapses, as have occurred on the flanks of the Hawaiian and Canary islands [*Moore et al.*, 1989; *Masson et al.*, 2002]. Plausible sources in the region of our study include big megathrust earthquakes every few hundred years [*Jankaew et al.*, 2008; *Sieh et al.*, 2008] and earthquakes on the Sumatran Fault [*Sieh and Natawidjaja*, 2000]. The frequency of large earthquakes from these sources (10^2 years) is much shorter than the frequency of our landslides (10^5 years), but this poses no problem, since the earthquakes can only provide a triggering mechanism when the delta is poised for a failure.

5.3. Landslide Hazard Assessment

[25] Large submarine landslides can involve many thousand km^3 of material, two to three orders of magnitude larger than any terrestrial landslide [*Hampton et al.*, 1996]. For example, the Storegga slide involved some 300 km^3 of sediment, affected 95,000 km^2 of the Norwegian slope and basin and had a run-out distance of around 800 km [*Haflidason et al.*, 2004].

[26] An important lesson from many other studies, however, is that a landslide's size is not necessarily proportional to the hazard it poses [*Masson et al.*, 2006]. Thus, in our case, we cannot just assume an intermediate tsunami hazard from our intermediate-sized submarine landslides. One reason for this caution is that continental-margin landslides that occur on very low slopes may translate basinward slowly by retrogressive processes, similar to quick-clay flows on land [*Prior and Coleman*, 1980; *Bentley and Smalley*, 1984]. Many such landslides appear to have limited tsunamigenic potential because they displace seawater slowly. Their principal threat may be to cables or other seabed installations.

[27] The speed of translation of the slides can be qualitatively assessed by examining their morphology for any indication of their momentum. One debris lobe of LS1 extends over an anticline, suggesting high-velocity transport (Figure 2). Careful inspection of the sediment geometry over the anticline, however, leads us to conclude that the LS1 debris flow likely occurred before the folding, or at near the initiation time of the folding. This is suggested by the greater thickness of the overlying sediment package directly atop LS1 deposits (between LS1 and MIS 6) upslope (SE) of the anticline. The thickened sediment packages suggest that the overlying sediments were laid down as folding was occurring. Unfortunately, the sediment reflectors beneath LS1 are poorly imaged, so one cannot assess if they also were deposited during anticline growth. The strata are too poorly resolved to determine with any confidence that the slide over-rode a pre-existing anticline at high velocity. Thus we cannot assess whether these slides were fast-moving, and thereby tsunamigenic.

[28] Another hazardous phenomenon that might have been associated with our submarine slides is turbidity currents. Turbidity currents are gravity flows in which sediment grains are maintained in suspension by fluid turbulence. Though initiated by a landslide, they can separate from the slide body and travel hundreds of km beyond the topographically obvious limits of the deposit. Turbidity currents can last several hours and have velocities as high as 20 m/s. Such currents have caused severe damage to submarine telecommunication cables (Western New Britain Trench, *Krause et al.* [1970]; 1929 Grand Banks earthquake, offshore Newfoundland, *Piper et al.* [1999]; 2006 Pingtung earthquake, Taiwan, *Hsu et al.* [2008]).

[29] Thin deposits associated with a turbidity current could well be impossible to resolve on the seismic lines we examined. Thus, the fact that we found no evidence of turbidity current deposits is no guarantee that they did not occur. However, it is likely that the slope angles (~1° down to 800 m, and ~0.15° at greater depth) are too low to have enabled such flows (Figure 1d). *Piper et al.* [1999] has pointed out that debris flows should pass through hydraulic jumps on steep slopes (in the case of the turbidity current after the 1929 Grand Banks earthquake, a change of slope from 6° to 10°) to transform into turbidity currents. The fact that our slopes decrease with depth suggests there would have been no accelerating mechanism for the landslide masses to generate turbidity currents.

5.4. Timing of Landslides

[30] According to the truncation relationships between headscarps and paleo-shoreline indicators, we believe the slides in the Malacca Strait-Mergui Basin shelf margin to have occurred during sea-level lowstands. This timing is quite different from what has been observed at higher latitudes. For example, the second Storegga landslide occurred during melt-water pulse 1C (8,200–7,600 BP), when sea level was rapidly rising to a position near the Holocene maximum level. There are several explanations as to why submarine landslides occurred during transgression rather than during glacial maxima, when sediment loading at continental slopes peaks. One explanation is that during the last glaciation, the sediment input to the Storegga area was merely modest (~100 m), compared to the penultimate glaciation. It was the excess pore pressure transferred from the North Sea Fan to the sliding area that triggered this megaslide, and this pore pressure transfer took several thousand years [*Bryn et al.*, 2005]. Another debated explanation is that gas hydrate dissociation during transgression may have weakened the strata involved in the slide, especially with evidence of bottom simulating reflectors in the north-eastern flank of the Storegga slide [*Mienert et al.*, 2005]. The last complementary explanation is that seismic shaking in northern Norway, the proposed triggering

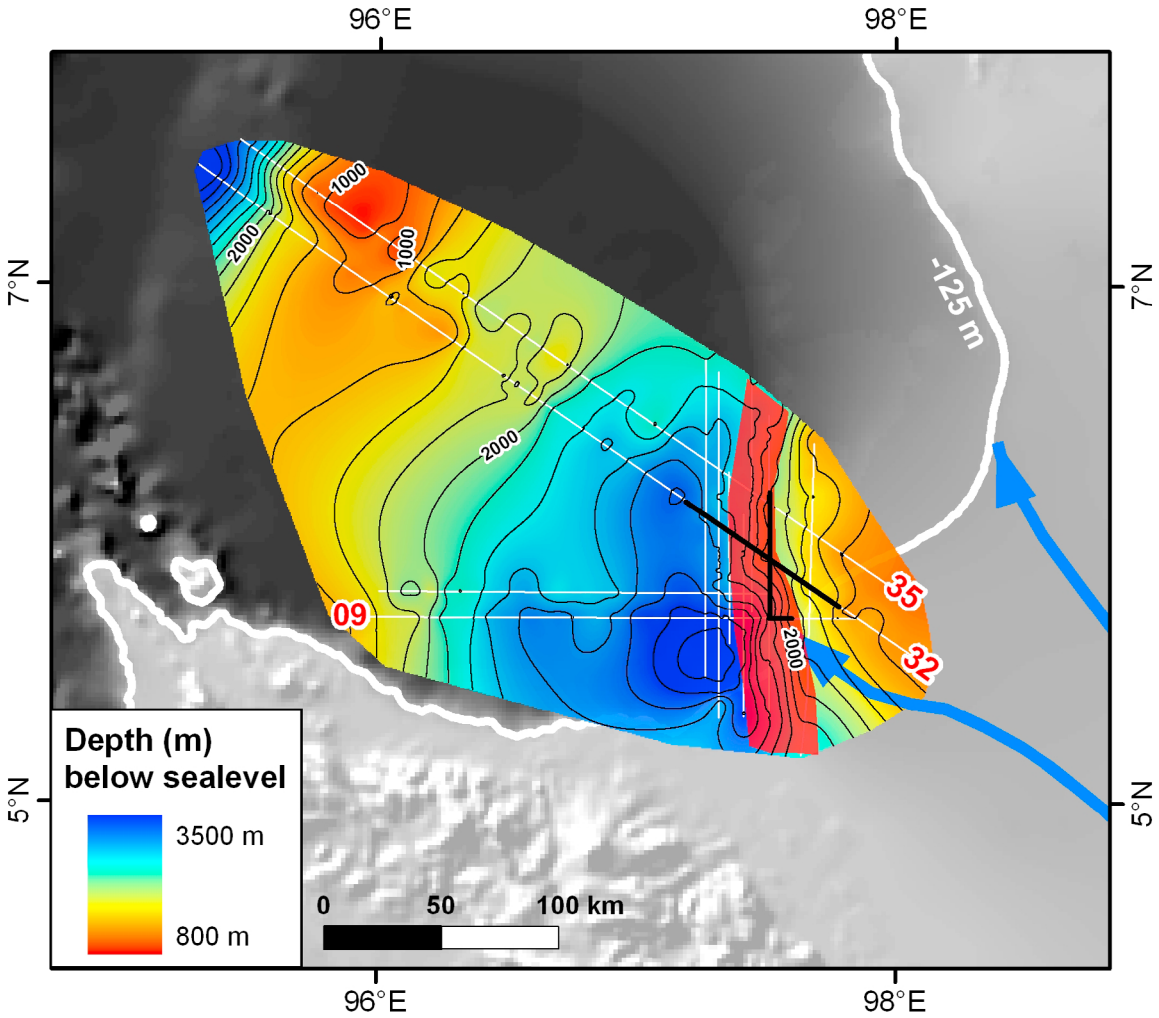

Figure A1. Isodepth map of the Late-Miocene unconformity in the Mergui Basin. Several industry drillholes (not shown here) as well as a dense grid of seimic profiles (not shown in this paper) are used to determine the depth (below sea level) of the Late-Miocene unconformity. Red zone represents a zone of west-dipping normal faults largely below the depth range shown in Figure 2. Thick black lines show the extent of seismic profiles in Figures 2 and A2. Note the increased depth of the Late-Miocene unconformity to the south.

mechanism for the sliding events, is mostly caused by earthquakes due to reactivation of the Late Jurassic-Early Cretaceous faults by post-glacial rebound [*Bungum and Lindholm*, 1998; *Fjeldskaar et al.*, 2000; *Bungum et al.*, 2005].

[31] The mechanisms for the Malacca Strait-Mergui Basin submarine slides are different. The regressive strata within which the slide occurred are more than 200 m thick. Although we can not completely rule out the possibility of excess pore pressure transfer from the delta at the outlet of the Malayan stream, this thick layer of sediment could well have produced adequate in-situ excess pore pressure to induce failure. There is no need for lag time between peak sedimentation and landsliding.

[32] Does gas hydrate dissociation also play a role to induce slides in this region? Bottom simulating reflector (BSR), characterized by sea-floor parallel reflector that cuts across normal sedimentary strata, is key to identifying the existence of gas hydrate. BSRs were reported below the seabed in the water depths of 850 to 2000 m in the Andaman Sea [*Sethi et al.*, 2004]. Since most of our study area was outside the gas hydrate stability zone during sea level lowstands, it is not likely that gas hydrate dissociation can be responsible for the sliding on the upper continental slope. The timing of sliding therefore does not depend on the warming up of sea water temperature during transgression.

[33] As for a seismic trigger, one would certainly not argue that the rupture of nearby active faults, such as the Sunda megathrust and the Sumatran Fault, is restricted to periods of sea-level trangression. There is no necessary coupling of such tectonic activity with glacial cycles. Even if a secondary or tertiary influence on fault activity were to be ascribed to hydrostatic loading during transgression of sea level in low latitudes, this would only modulate the otherwise more or less steady mechanism of tectonic strain accumulation and relief. The causes of the Malacca Strait-Mergui Basin slides are likely quite simple: Spatiotemporal variations of peak sediment influx near the shelf margin

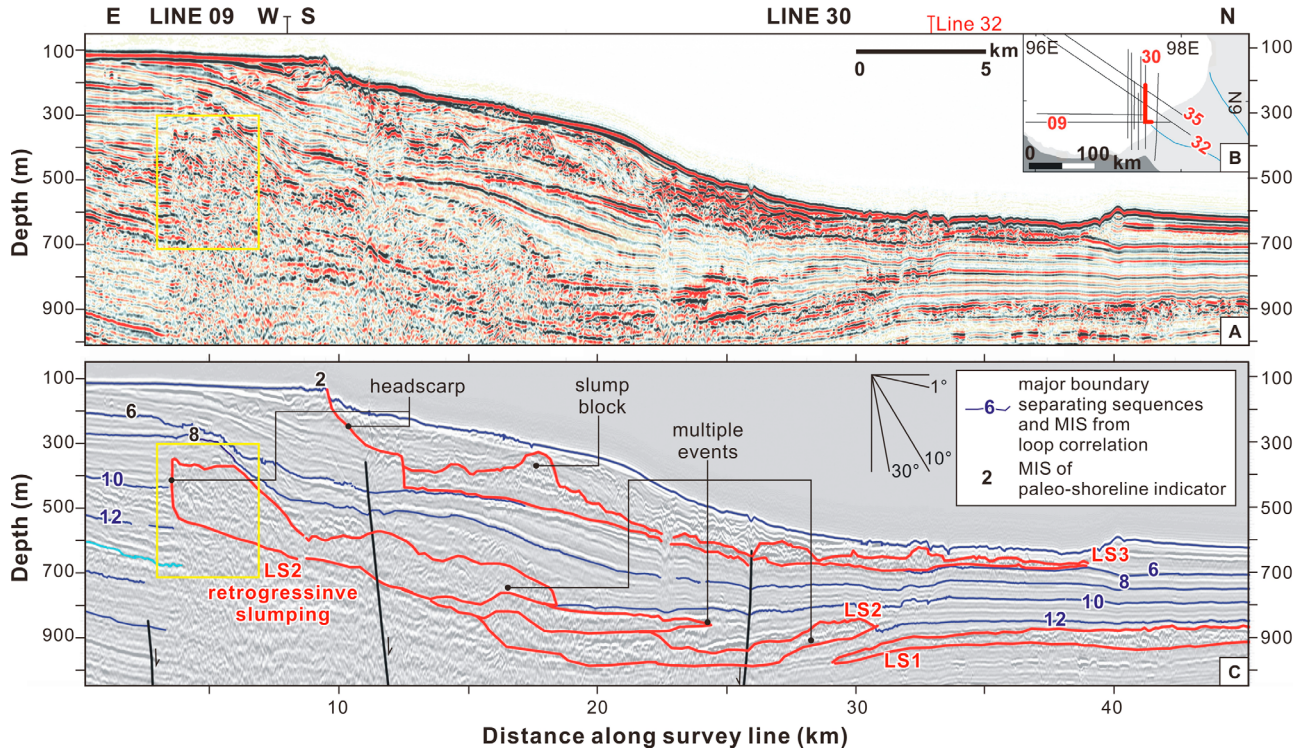

Figure A2. (a) Seismic profile Line 09–Line 30. Nails mark intersections of cross lines. See Figure A2b for profile location. Yellow box is for referencing between original and interpreted profiles. (c) Interpreted profile of Figure A2a. Black numbers (2, 6, and 8 at left side of profile) are the marine isotope stages of the identifiable paleo-shoreline indicators in this profile. Blue numbers (elsewhere) are the marine isotope stages of regression/transgression boundaries (dark blue lines) from loop correlation. Landslides are outlined in thick red lines. (d) Northern extension of profile in Figure A2a. (e) Northern extension of interpreted profile in Figure A2c.

during sea-level lowstands combined with seismic triggering. We do not know yet if this simple combination of mechanisms caused most or all other low-latitude shelf-margin landslides, but it seems quite certain that the factors that control the basin-margin instability in high latitudes is more complex than those that are important in low latitudes.

[34] Most important is our conclusion that the potential for a submarine landslide similar to the ones we have described is quite low during sea level high stands as has been the case throughout the past many thousand years, because sediments are not being deposited rapidly at the shelf margin.

6. Conclusion

[35] Three very large submarine landslides have occurred on the continental shelf separating the Andaman Sea and the Malacca Strait during lowstands of sea level about 20–30, 342–364 and 435–480 kyr ago. Rapid sediment deposition on the shelf margin during sea-level lowstands is an essential precondition for basin-margin submarine landsliding there. Spatiotemporal variations of sediment supply due to lobe switching or Asian monsoon intensity may further enhance or impede landslide occurrence during lowstands. Once these preconditions have been met, seismic shaking could serve as a triggering mechanism. We cannot provide any solid evidence for high emplacement velocities and, thus, the tsunamigenic capacity of these landslides. Nonetheless, the lack of rapid deposition on the continental slope during the current Holocene sea-level highstand may preclude the possibility of another very large submarine slide in this location until the next glacially induced lowstand, thousands or tens of thousands of years in the future.

Appendix A: Tectonic Subsidence of the Mergui Basin Since the Late Miocene

[36] We use several industry drillholes (not shown here) as well as a dense grid of seismic profiles (not shown in this paper) to construct the isodepth map (below sea level) of the Late Miocene unconformity (Figure A1). Its depth is constrained and time-depth converted by using an industrial borehole near the center of Mergui Basin, and cross-traced in a denser network of 2D seismic lines than what are used in this study. The derived isodepth map agrees with the depth of the Late Miocene unconformity from E-1 well in *Polachan and Racey* [1994]. The reflectors of the unconformity are of greater depth and therefore are not shown in all our figures. The basin submerged along a normal fault system along its eastern boundary (wide red zone of Figure A1). The strike of the normal fault system depicted here is only approximate; its actual location is not very well

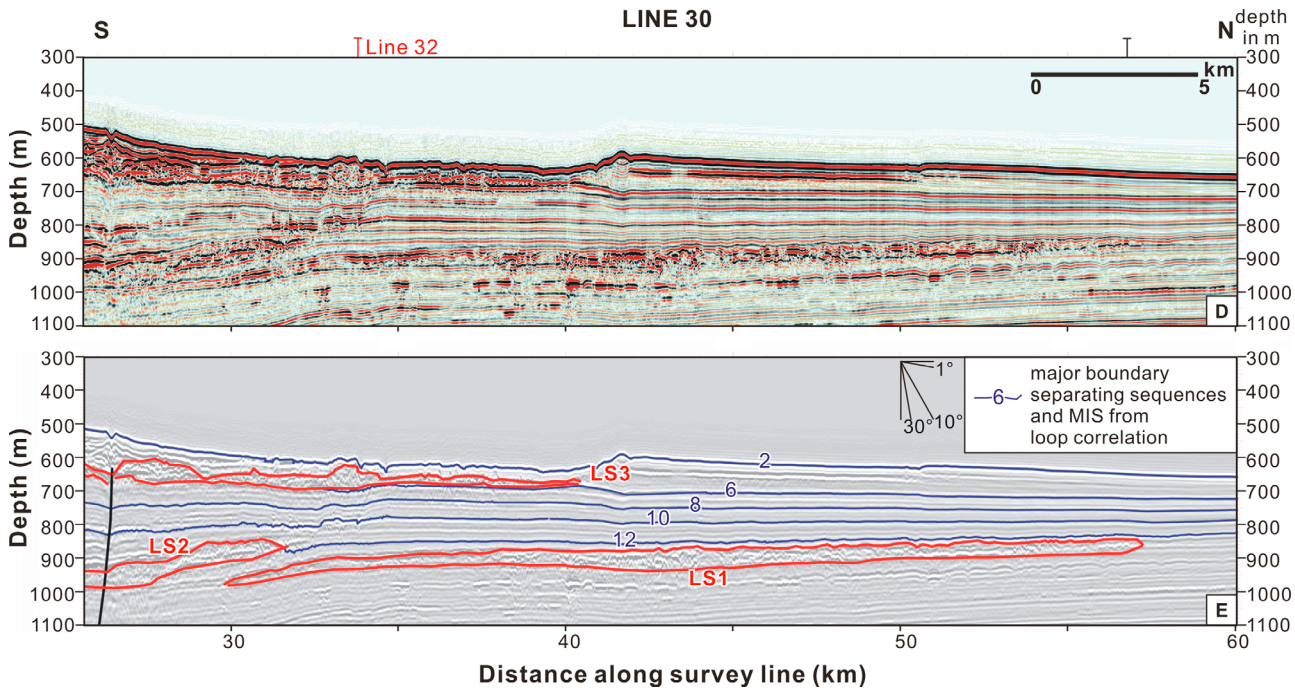

Figure A2. (continued)

determined, due to uncertainties in connecting normal faults across 2D seismic profiles. A normal separation across this fault increases from ~800 m in the north to 1200 ~ 1400 m in the south, implying maximum subsidence center near the southern part of the Mergui Basin. To avoid confusion, we caution that the Late-Miocene unconformity and the major normal system are mostly beyond the depth of the seismic profiles shown in this paper (Figures 2 and A2).

Appendix B: Retrogressive Slumping Events of LS2

[37] LS2 is composed of multiple events based on three major observations. First, the debris lobe of LS2 underlies the regression/transgression boundary of MIS 10 (Figure 2c, 30 km), whereas the headscarp of LS2 has eroded away the paleo-shoreline indicator of MIS 10 and part of the regression sequences beneath MIS 8 (Figure A2c, 4 km). This yields age inconsistency if the debris lobe in Figure 2c and the headscarp were to be formed synchronously. Second, there are continuous reflectors sandwiched in between the lower two debris lobes (Figure A2c, 22–25 km), implying the two lobes were formed separately. Third, the latest slump of LS2 has reflectors that bend to override the underlying debris lobe (Figure A2c, 17 km). Therefore, we interpret LS2 to be composed of three subslides. The main event is the lowermost debris lobe which can be traced in most of the seismic lines. The later two may be retrogressive slumping of the first one, with the headscarp preserved only near the intersection of seismic Lines 09 and 30.

[38] **Acknowledgments.** We thank Petroleum Geo-Services (PGS), Asia Pacific center in Singapore for providing the seismic reflection profiles used in this study. We also thank Seismic Micro-Technology (SMT) for providing to Caltech a university grant for the Kingdom Suite software used to process these data and generate figures. This project was funded by a grant from the Earth Observatory of Singapore (EOS grant number M61580001) and is EOS Contribution Number 5. Tectonic Observatory Contribution Number 135.

References

Asku, A. E., R. N. Hiscott, and D. Yasar (1999), Oscillating water levels of the Marmara Sea and vigorous outflow into the Aegean Sea from Marmara Sea-Black Sea drainage corridor, *Mar. Geol.*, *153*, 275–302.

Bentley, S. P., and I. J. Smalley (1984), Landslips in sensitive clays, in *Slope Instability*, edited by D. Brunsden and D. B. Prior, pp. 457–490, Wiley, Chichester, UK.

Bugge, T., S. Befring, R. Belderson, T. Eidvin, E. Jansen, N. Kenyon, H. Hotedahl, and H. Sejrup (1987), A giant three-stage submarine slide off Norway, *Geo Mar. Lett.*, *7*, 191–198.

Bugge, T., R. Belderson, and N. Kenyon (1988), The Storegga slide, *Phil. Trans. R. Soc. A*, *325*, 357–388.

Bryn, P., K. Berg, C. F. Forsberg, A. Solheim, and T. J. Kvalstad (2005), Explaining the Storegga Slide, *Mar. Pet. Geol.*, *22*, 11–19.

Bungum, H., and C. Lindholm (1998), Seismo- and neotectonics in Finnmark, Kola Peninsula and the Southern Barents Sea. Part 2: seismological analysis and seismotectonics, *Tectonophysics*, *270*, 15–28.

Bungum, H., C. Lindholm, and J. I. Faleide (2005), Post-glacial seismicity offshore mid-Norway with emphasis on spatio-temporal-magnitudal variations, *Mar. Pet. Geol.*, *22*, 11–19, doi:10.1016/j.marpetgeo.2004.10.007.

Curray, J. R. (2005), Tectonic and history of the Andaman Sea region, *J. Asian Earth Sci.*, *25*, 187–232.

Emery, K. (1971), Bottom sediment map of Malacca Strait, *Tech. Bull.*, *Ecafe*, 149–152

Emmel, F. J., and J. R. Curray (1982), A submerged Late Pleistocene delta and other features related to sea level changes in the Malacca Strait, *Mar. Geol.*, *46*, 197–216.

Evans, D., et al. (2005), Palaeoslides and other mass failures of Pliocene to Pleistocene age along the Atlantic continental margin of NW Europe, *Mar. Pet. Geol.*, *22*, 1131–1148.

Fjeldskaar, W., C. Lindholm, J. Dehls, and I. Fjeldskaar (2000), Postglacial uplift, neotectonics and seismicity in Fennoscandia, *Quat. Sci. Rev.*, *19*, 1413–1422.

Haflidason, H., H. Sejrup, I. Berstad, A. Nygard, T. Richter, and R. Lien (2003), A weak layer feature on the northern Storegga slide escarpment, in *European Margin Sediment Dynamics*, edited by K. Berg et al., pp. 55–62, Springer.

Haflidason, H., H. Sejrup, A. Nygard, J. Mienert, P. Bryn, R. Lien, C. Forsberg, K. Berg, and D. Masson (2004), The Storegga Slide: architecture, geometry and slide development, *Mar. Geol.*, *213*, 201–234.

Hampton, M. A., H. J. Lee, and J. Locat (1996), Submarine landslides, *Rev. Geophys.*, *34*, 33–59.

Hsu, S.-K., J. Kuo, C.-L. Lo, C.-H. Tsai, W.-B. Doo, C.-Y. Ku, and J.-C. Sibuet (2008), Turbidity currents, submarine landslides and the 2006 Pingtung earthquake off SW Taiwan, *Terr. Atmos. Ocean Sci.*, *19*, 767–772.

Jankaew, K., B. F. Atwater, Y. Sawai, M. Choowong, T. Charoentitirat, M. E. Martin, and A. Prendergast(2008), Medieval forewarning of the 2004 Indian Ocean tsunami in Thailand, *Nature*, *455*, 1228–1231.

Kamesh Raju, K.A., T. Ramprasad, P.S. Rao, B. Ramalingeswara Rao, and J. Varghese (2004), New insights into the tectonic evolution of the Andaman basin, northeast Indian Ocean, *Earth Planet. Sci. Lett.*, *221*, 145–162.

Keller, G. H., and A. F. Richards (1967), Sediments of the Malacca Strait, southeast Asia, *J. Sediment. Petrol.*, *37*, 102–127.

Krause, D. C., W. C. White, D. J. W. Piper, and B. C. Heezen (1970), Turbidity currents and cable breaks in the Western New Britain Trench, *Geol. Soc. Am. Bull.*, *81*, 2153–2160.

Kvalstad, T. J., L. Andresen, C. F. Forsberg, K. Berg, P. Bryn, and M. Wangen (2005), The Storegga slide: evaluation of triggering sources and slide mechanics, *Mar. Pet. Geol.*, *22*, 245–256.

Laberg, J. S., T. O. Vorren, J. Mienert, H. Haflidason, P. Bryn, and R. Lien (2003), Preconditions leading to the Holocene Traenadjupet slide, offshore Norway, in *Submarine Mass Movements and Their Consequences*, edited by J. Locat and J. Mienert, pp. 247–254, Kluwer Acad., Dordrecht, Netherlands.

Masson, D. G., A. B. Watts, M. J. R. Gee, R. Urgeles, N. C. Mitchell, T. P. L. Bas, and M. Canals (2002), Slope failures on the flanks of the western Canary Islands, *Earth Sci. Rev.*, *57*, 1–35.

Masson, D. G., C. B. Harbitz, R. B. Wynn, G. Pedersen, and F. Løvholt (2006), Submarine landslides: processes, triggers and hazard prediction, *Phil. Trans. R. Soc. A*, *364*, 2009–2039.

Métivier, F., Y. Gaudemer, P. Tapponnier, and M. Klein (1999), Mass accumulation rates in Asia during the Cenozoic, *Geophys. J. Int.*, *137*, 280–318.

Mienert, J., S. Bünz, S. Guidard, M. Vanneste, and C. Berndt (2005), Ocean bottom seismometer investigations in the Ormen Lange area offshore mid-Norway provide evidence for shallow gas layers in subsurface sediments, *Mar. Pet. Geol.*, *22*, 287–297.

Moore, J. G., D. A. Clague, R. T. Holcomb, P. W. Lipman, W. R. Normark, and M. E. Torresan (1989), Prodigious submarine landslides on the Hawaiian ridge, *J. Geophys. Res.*, *94*, 17,465–17,484.

O'Leary, D. W. (1991), Structure and morphology of submarine slab slides: Clues to origin and behavior, *Mar. Geotechnol.*, *10*, 53–69

Piper, D. J., P. Cochonat, and M. L. Morrison (1999), The sequence of events around the epicentre of the 1929 Grand Banks earthquake: initiation of debris flows and turbidity current inferred from sidescan sonar, *Sedimentology*, *46*, 79–97.

Prell, W. L., J. Imbrie, D. G. Martinson, J. J. Morley, N. G. Pisias, N. J. Shackleton and H. F. Streeter (1986), Graphic correlation of oxygen isotope: stratigraphy application to the late Quaternary, *Paleoceanography*, *1*, 137–162.

Prior, D. B., and J. M. Coleman (1980), Active slides and flows in underconsolidated marine sediments on the slopes of the Mississippi Delta, in *Marine Slides and other Mass Movements*, edited by S. Saxov and J. Nieuwenhuis, pp. 21–50, Plenum.

Polachan, S., and A. Racey (1994), Stratigraphy of the Mergui Basin, Andaman Sea: Implications for petroleum exploration, *J. Pet. Geol.*, *17*, 373–406.

Rabineau, M., S. Berné, D. Aslanian, J. Olivet, P. Joseph, F. Guillocheau, J. Bourillet, E. Ledrezen, and D. Granjeon (2005), Sedimentary sequences in the Gulf of Lion: a record of 100,000 years climatic cycles, *Mar. Pet. Geol.*, *22*, 775–804.

Rabineau, M., S. Berné, J. Olivet, D. Aslanian, F. Guillocheau, and P. Joseph (2006), Palaeo sea levels reconsidered from direct observation of paleoshoreline position during Glacial Maxima (for the last 500,000 yr), *Earth Planet. Sci. Lett.*, *252*, 119–137.

Sethi, A. K., A. V. Sathe, and M. V. Ramana (2004), Potential natural gas hydrate resources in Indian offshore areas, paper presented at the AAPG Hedberg Conference "Gas hydrates: Energay resources potential and associated geologic hazards", Vancouver, BC, Canada.

Sieh, K., and D. Natawidjaja (2000), Neotectonics of the Sumatran fault, Indonesia, *J. Geophys. Res.*, *105*, 28,295–28,326.

Sieh, K., D. H. Natawidjaja, A. J. Meltzner, C. C. Shen, H. Cheng, K. S. Li, B. W. Suwargadi, J. Galetzka, B. Philibosian, and R. L. Edward (2008), Earthquake supercycles inferred from sea-level changes recorded in the corals of west Sumatra, *Science*, *322*, 1674–1678.

Singh, S. C., et al. (2008) Seismic evidence for broken oceanic crust in the 2004 Sumatra earthquake epicentral region, *Nat. Geosci.*, *1*, 777–781.

von Blanckenburg, T. Hewawasam, and P. W. Kubik (2004), Cosmogenic nuclide evidence for low weathering and denudation in the west, tropical highlands of Sri Lanka, *J. Geophys. Res.*, *109*, F03008, doi:10.1029/2003JF000049.

Wang, P. (1999), Response of Western Pacific marginal seas to glacial cycles: paleoceanographic and sedimentological features, *Mar. Geol.*, *156*, 6–39.

Whiting, B. M., G. D. Karner, and N. W. Driscoll (1994), Flexural and stratigraphic development of the west Indian continental margin, *J. Geophys. Res.*, *99*(B7), 13,791–13,811.

Zhang, Y. G., J. Ji, W. L. Balsam, L. Liu, and J. Chen (2007), High resolution hematite and goethite records from ODP 1143, South China Sea: co-evolution of monsoonal precipitation and El Nino over the past 600,000 years, *Earth Planet. Sci. Lett.*, *264*, 136–150.

Y. N. Lin and J. Stock, Geological and Planetary Sciences, California Institute of Technology, MC100-23, 1200 E California Blvd., Pasadena, CA 91101, USA. (ninalin@caltech.edu)

K. Sieh, Earth Observatory of Singapore, Nanyang Technological University, 50 Nanyang Avenue, Singapore.